JOURNAL OF SPACECRAFT AND ROCKETS
Vol. 34, No. 1, January–February 1997

Large-Scale Roughness Influence on Turbulent Hypersonic Boundary Layers Approaching Compression Corners

H. Babinsky*
Cranfield University, Cranfield MK43 OAL, England, United Kingdom
and
J. A. Edwards†
Defence Research Agency, Fort Halstead, Sevenoaks TN14 7BP, England, United Kingdom

The influence a short stretch of large-scale regular surface roughness on a Mach 5 turbulent boundary layer approaching a compression corner was investigated on axisymmetric wind-tunnel models. Roughnesses were of sawtooth and cavity shape with typical dimensions up to a full boundary-layer thickness. The effects of roughness on flow parameters compared to an equivalent smooth surface differed significantly for each measured quantity. Velocity profiles downstream of the roughness were found to be less full, and skin friction was reduced. Surface heat flux was increased for a short distance. Surface pressures remained unchanged. Little influence was noted on the flow in the compression corner. Upstream influence was increased in some cases but no large-scale separation due to the additional effects of roughness was observed. Roughnesses of sawtooth shape were found to cause greater disturbance to the flow than square cavities.

Nomenclature

$c_{d,r}$ = drag coefficient for rough surface
$c_{d,s}$ = drag coefficient for smooth surface
c_f = skin-friction coefficient
p_{res} = reservoir pressure
p_w = surface pressure
$\dot{q}$ = surface heat transfer
U = streamwise velocity component
U^+ = streamwise velocity in law-of-the-wall coordinates
X = streamwise coordinate
Y = surface distance
Y^+ = surface distance in law-of-the-wall coordinates
Δd = roughness drag contribution, defined in text
δ_0 = smooth wall boundary-layer thickness at $X = -50$ mm

Introduction

SMALL-SCALE irregular surface roughness has been investigated widely in subsonic, supersonic and hypersonic flow, but the problem discussed here is of a different category, as illustrated by a typical application, a hypersonic projectile as shown in Fig. 1. It can be seen that an area of rather large thread-like roughness exists in the center of the cylindrical part of the projectile. These buttress threads are necessary to allow the projectile to be housed in an outer shell (sabot), which transmits the acceleration forces during the firing from a gun. Once the projectile leaves the gun barrel, aerodynamic forces split the sabot and it is removed from the projectile. The flight of such projectiles is usually at sea level and very high velocities, entering the hypersonic regime. The boundary layer over most of the projectile surface is turbulent. The buttress threads are of the order of a boundary-layer thickness in depth and, therefore, have a significant impact on the flow in this region. There are usually control surfaces or stabilizers, such as fins or flares, downstream of this roughness. These elements are the origin of regions of adverse pressure gradients and can cause flow separation.

This configuration poses a number of aerodynamic problems that are addressed in this paper. The oncoming turbulent boundary-layer characteristics are changed due to the stretch of roughness. On the following smooth section the boundary-layer profile is expected to relax before encountering an adverse pressure gradient. Depending on the changes to the profile due to the roughness and the subsequent relaxation, the flow in the corner interaction can differ significantly from a smooth wall case. It has been shown in previous investigations[1,2] that the addition of roughness can lead to separation in an otherwise attached compression corner. However, these results were obtained with roughness stretching along the whole surface and through the compression corner, whereas the problem considered here is more complex. Two particular aspects are investigated experimentally: the relaxation of the boundary layer after a stretch of roughness and the behavior of a boundary layer modified by roughness as it enters a region of adverse pressure gradient, modeled by a compression corner. The distance between the end of the roughness and the compression corner was kept constant ($\approx 5\delta_0$), while the type and height of the roughness has been varied.

Apparatus and Measurement Techniques

All experiments were performed in the Defence Research Agency (DRA) Fort Halstead supersonic wind tunnel (High Super Sonic Tunnel; HSST). This facility is a supersonic intermittent pressure vacuum tunnel. In the configuration used here it features a contoured axisymmetric nozzle with a centerbody, giving a useful flow area with a diameter of 0.2 m. The flow conditions were set to give a total pressure of 716×10^3 N/m^2, a total temperature of 400 K, and a freestream Reynolds number of 13×10^6 m^{-1}, at a Mach number of 5.07. The undisturbed centerbody boundary-layer thickness at the nozzle exit was found to be 9.8 mm, with a skin-friction coefficient of 0.9×10^{-3}.

To allow for comparison with computational fluid dynamics (CFD) predictions, a detailed survey of the nozzle flow has been conducted and is presented in Ref. 3. During this investigation, it

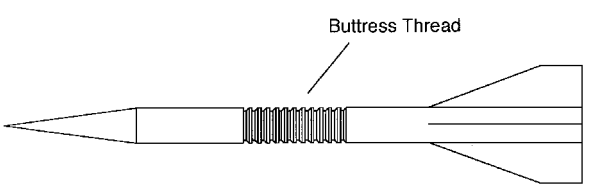

Fig. 1 Simplified drawing of a generic projectile, showing the location and relative size of the buttress thread.

Presented as Paper 95-0334 at the AIAA 33rd Aerospace Sciences Meeting, Reno, NV, Jan. 9–12, 1995; received Jan. 19, 1995; revision received Aug. 12, 1996; accepted for publication Sept. 24, 1996.

*Research Assistant, College of Aeronautics; currently Lecturer, Department of Engineering, University of Cambridge, Cambridge CB2 1PZ, England, United Kingdom.
†Senior Principal Consultant, WX7 Division. Senior Member AIAA.

was found that the operating conditions vary between different experiments and throughout a single run for the same wind-tunnel settings. These variations amounted to 12% in total pressure and 10% in total temperature. The influence of these variations on pressure measurements is removed by normalizing all measured pressures with a simultaneously recorded settling chamber pressure. A comparison of heat transfer results, however, has to take into account the influence of varying operating conditions.

The measurements include surface pressure and heat transfer measurements, as well as boundary-layer pitot traverses. Surface pressure transducers of the type Kulite® XCS-062-15A have been mounted inside the model, as close to the surface as possible. The hole diameter at the surface was 0.5 mm. Boundary-layer profiles have been performed with a traversing probe. It was found that response time problems influenced the measurements very close to the surface, and introduced additional uncertainties. This area of restricted accuracy is limited to 0.5 mm from the surface. To obtain velocity profiles from the pitot-pressure measurements, the Mach number has been calculated by assuming constant static pressure throughout the boundary layer and measuring the wall pressure at the profile location. The temperature profile has been derived using Crocco's velocity–temperature correlation. These assumptions introduce significant uncertainties into the boundary-layer velocity profiles and these data are therefore not recommended for CFD code validation. For this purpose all measured pitot-pressure profiles are given in Ref. 3.

Surface heat transfer has been measured on the complete model surface using liquid crystal thermography. This method supplies data of a spatial resolution superior to traditional techniques. The developments leading to its use in the HSST were first described in Babinsky and Edwards.[4] Further details can be found in Ref. 5.

An analysis of all experimental errors has been presented,[3] and the results are summarized as follows (at 100:1 odds): surface/wall pressures ±4%, total temperatures ±3%, surface heat flux ±8%, pitot pressures in freestream ±0.5%, pitot pressures in boundary layer ±0.5%–±3%, and velocity profiles ±15% (outside pressure gradient regions).

Models and Configurations

The models used in this study were designed to fit onto the centerbody of the Mach 5 nozzle, which is held with struts inside the subsonic settling chamber. The centerbody is of a circular cross section with a diameter of 50 mm, and it provides a sufficiently long length to naturally grow a turbulent boundary layer of approximately 10 mm thickness. A general layout of the model is shown in Fig. 2. A mounting shaft is connected to the end of the centerbody, which can be fitted with a variety of modules, as shown in Fig. 3. A typical configuration contains a region of roughness followed by a smooth surface and a flare modeling the adverse pressure gradient region. Flare angles were chosen to be 15 and 20 deg. Both were not expected to separate the boundary layer with the larger flare angle being very close to the expected angle of incipient separation. All measurements are presented in a coordinate system originating at the junction between cylinder and flare, as shown in Fig. 4. All roughness types investigated end 50 mm upstream of the corner ($X = -50$ mm).

The models were manufactured of black Ertalyte, which is the trade name for a thermoplastic polyester based on polyethylene terephtalate (PETP). It was chosen for its good machinability and strength as well as thermal coefficients making it suitable for liquid crystal thermography in this facility. The physical properties have been obtained from the manufacturer and checked by DRA Fort Halstead.

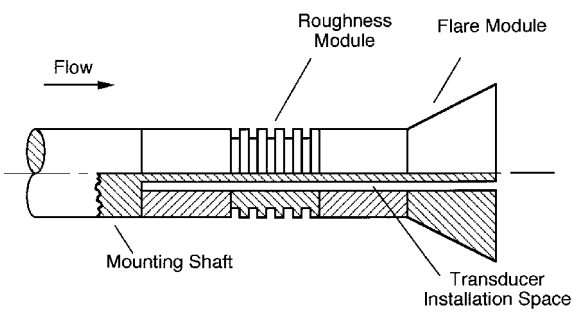

Fig. 2 Roughness and compression corner model in the HSST.

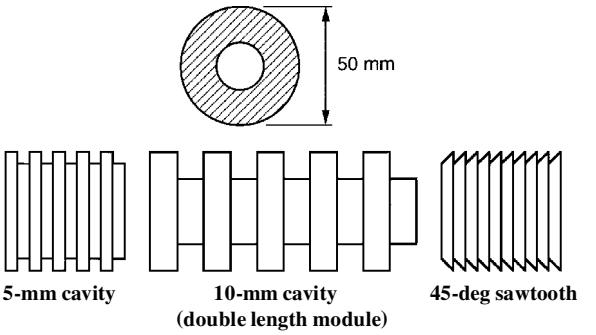

Fig. 3 Available roughness modules.

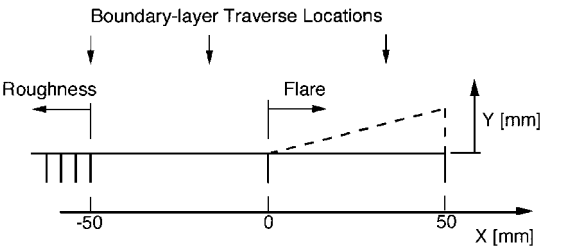

Fig. 4 Coordinate system and boundary-layer traverse positions.

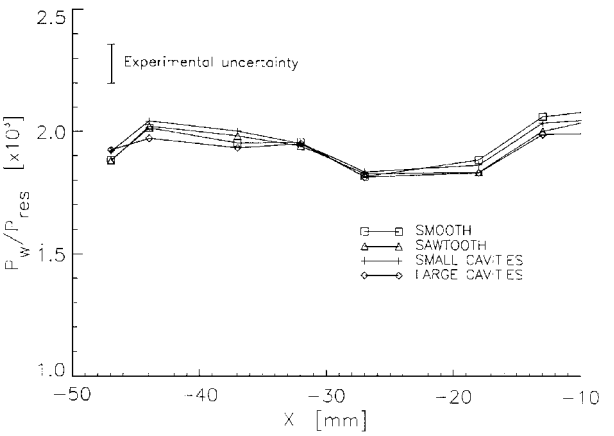

Fig. 5 Surface pressures downstream of the roughness modules.

Surface Pressure Measurements

Figure 5 shows the pressures recorded immediately downstream of the last roughness element normalized by the total pressure as earlier given. Within the accuracy of the measurements there is no difference in the results between the various types of roughness and the undisturbed wall pressure.

The next item investigated is the influence of the roughnesses on the flow in the compression corner. Figures 6 and 7 show the results obtained for both flare angles. The inviscid pressures for a 15- and a 20-deg cone are also given for comparison. To give a feeling for the length scales, the thickness of the undisturbed boundary layer δ_0 is indicated. Both cases show a pressure rise on the flare without reaching a plateau. The maximum pressures observed are below the inviscid levels. This suggests that the interaction extends farther downstream than the last measured position. This was confirmed by schlieren observations showing the corner shock to be still partly embedded in the boundary layer at this location. Both cases reveal a decrease in the pressures on the flare due to roughness. The sawtooth roughness shows the greatest effect, whereas the small cavities cause only a small difference from the smooth wall case. For both cases the maximum reduction of pressures, caused by the sawtooth roughness, is approximately 7%.

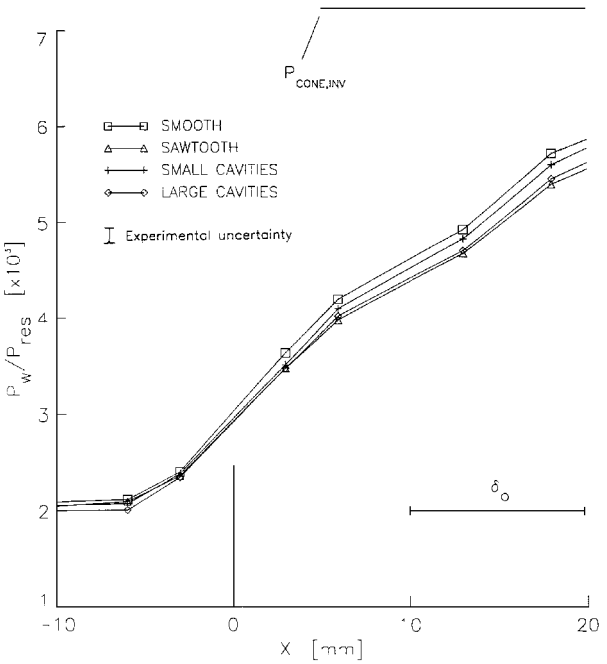

Fig. 6 Surface pressures on cylinder and 15-deg flare.

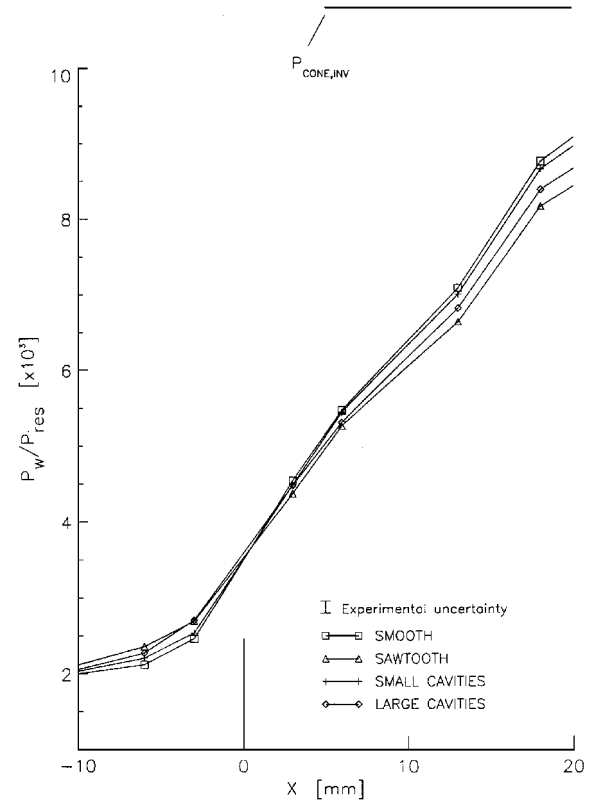

Fig. 7 Surface pressures on cylinder and 20-deg flare.

The pressures measured immediately upstream of the corner show a different behavior for the two flare angles. In the case of the 15-deg flare, no differences due to the roughnesses are noticeable within the accuracy of the measurements. In the case of the 20-deg flare, an increase in upstream pressures can be observed. This indicates an upstream movement of the shock/boundary-layer interaction. Again, the largest effect is seen for the sawtooth roughness.

An earlier investigation into the influence of roughness on the turbulent compression corner performed by Disimile and Scaggs[1] has found a more significant change in flow structure due to roughness, even for flows that are unseparated in the smooth case. A major difference between their work and the experiments reported here is that the roughness stretched all of the way through the interaction. The results obtained here indicate a substantial relaxation of the boundary layer over the short distance ($5\delta_0$) between the roughness and the corner.

Boundary-Layer Profiles

Mean pitot-pressure profiles have been recorded for all combinations of roughnesses and flare angles at eight streamwise positions. Only a selection will be presented here; the locations are indicated in Fig. 4.

Figures 8 and 9 show the measured velocity profiles at two locations downstream of the roughness elements. It can be seen that the roughnesses cause the boundary layers immediately downstream ($X = -50$) to be less full, with the sawtooth roughness having the greatest and the small cavities having the least effect. The velocities near the wall have been reduced, up to 20% in the case of the sawtooth roughness. The boundary-layer thickness is increased by 3%. Comparing the profiles obtained farther downstream it can be seen that the smooth wall boundary layer remains unchanged, whereas the profiles obtained behind the roughnesses become fuller with increasing distance from the end of the roughness element. Differences between profiles reduce. The velocities at the outer edge of the boundary layer show virtually no variations.

The profiles of Fig. 8 are also plotted in log-law coordinates compared with the law of the wall in Fig. 10. The values of skin friction necessary to determine the shear velocities have been obtained from fitting velocities to a theoretical family of profiles derived by Mathews et al.[6] based on the law of the wall and Coles' law of the wake. This assumes that the theoretical profile is valid for boundary layers distorted by the roughness. As all measurements are taken on a smooth surface, it is believed that this approach is valid. As a result, the profiles agree in the log-law region and exhibit differences in the wake strength. All profiles depart from the log law at a Y^+ of about 50. The profiles recorded downstream of the sawtooth roughness show the greatest deviation, thus indicating a large wake parameter. With increasing distance from the roughness end, the wake

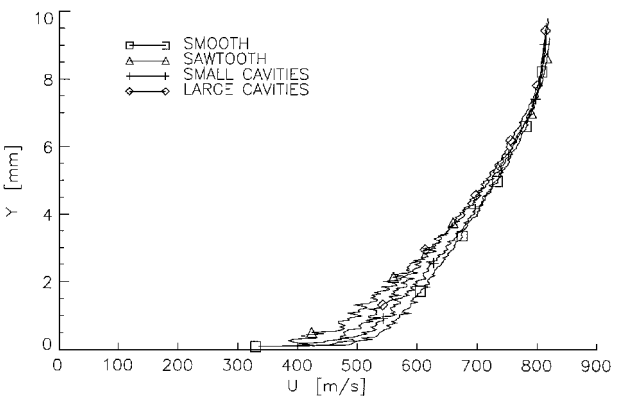

Fig. 8 Boundary-layer velocity profiles immediately behind the roughness, $X = -50$ mm.

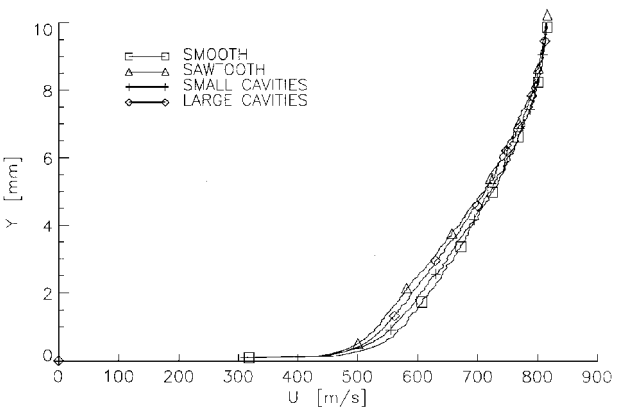

Fig. 9 Boundary-layer velocity profiles 32 mm behind the roughness, $X = -18$ mm.

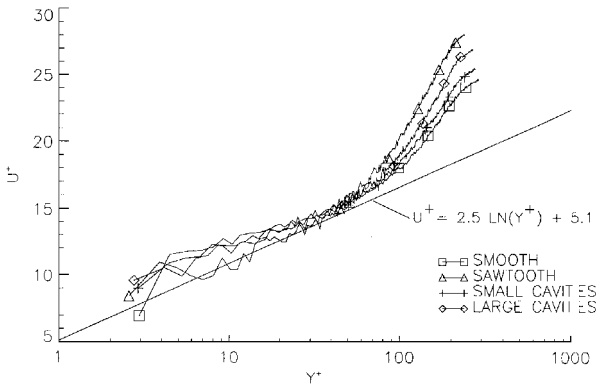

Fig. 10 Boundary-layer profiles in law-of-the-wall coordinates immediately behind the roughness, $X = -50$ mm.

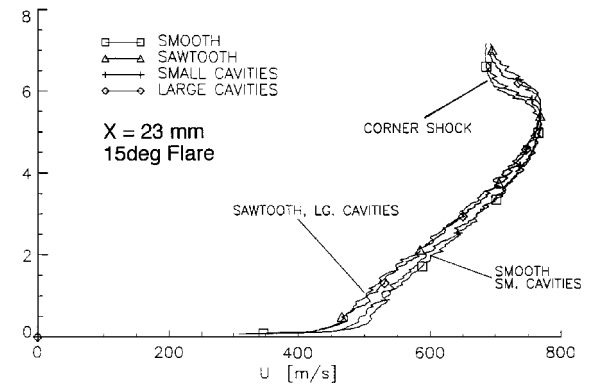

Fig. 11 Boundary-layer velocity profiles on the flare.

strengths reduce for the rough profiles, whereas the smooth wall profile remains unchanged. The skin-friction values obtained from fitting the velocity measurements to the theoretical profiles indicate a reduction due to roughness of up to 20% in the sawtooth case immediately behind the last roughness element. With increasing downstream distance, the differences caused by roughness reduce as the profiles relax toward the smooth wall boundary layer.

The effect of roughness on the velocity profiles was found to persist for many boundary-layer thicknesses downstream. This can be seen in Fig. 11, showing the velocity profiles at the farthest measurement location on the 15-deg flare. Whereas the differences between the profiles have reduced, they can still be clearly distinguished even after the shock/boundary-layer interaction. The location of the corner shock is indicated by the apparent decrease of velocities at the outer edge of the boundary layer. The velocities here are computed erroneously as the shock causes a change in static pressure. The true velocities at these locations are increasing. It can be seen that the compression wave system has been displaced away from the wall by approximately 0.7 mm due to the larger roughnesses. This value is considerably larger than the increase in oncoming boundary-layer thickness. This suggests that the upstream influence of the interaction has increased, and that the formation of the corner shock takes place earlier.

By comparing the velocity profiles obtained downstream of the roughness with the corresponding smooth wall profile, the momentum deficit due to roughness can be obtained. Normalizing this value with the length of the roughness and the freestream parameters provides an estimate of the additional drag caused by roughness compared to the skin-friction drag on a smooth surface. An estimate of the smooth wall drag can be obtained by using the value of skin friction obtained from the velocity profiles and assuming a constant skin-friction coefficient over the area of interest. The relative additional drag due to a stretch of roughness is

$$\Delta d = \frac{c_{d,r} - c_{d,s}}{c_{d,s}}$$

The results are subject to large uncertainties due to the assumptions in the velocity calculations and the experimental errors involved. Nevertheless they are given here to provide an additional insight into the effects of roughness: sawtooth Δd 2.1, small cavities Δd 0.6, and large cavities Δd 0.8, with $c_{d,s}(c_f)$ 0.9×10^{-3}.

It can be seen that the sawtooth shaped roughness causes the largest relative increase in drag and the small cavities have the least effect, which agrees with the changes seen in the velocity profiles. A question arising at this point is whether the mechanism is causing the drag. On the smooth surface this is obviously due to surface skin friction and $c_{d,s}$ is more correctly described as c_f. For the rough wall measurements, this is not true; in fact, the measurements downstream of the roughness indicate a reduction in skin friction. It is, therefore, plausible to assume that the dominant portion of the drag of large-scale surface roughness is caused by profile drag. This has also been concluded by Monta and Czarnecki,[2] who investigated smaller two-dimensional roughness in supersonic Mach numbers.

Surface Heat Transfer

The heat flux onto the surface has been measured using liquid crystal thermography[3–5] for all configurations. The data shown here are the result of averaging over a small strip along the middle of the model to give the streamwise variation and reduce random pixel noise. Because of variations in wind-tunnel operating conditions the level of heat transfer for each experiment varies. In theory, this variation could be removed by nondimensionalizing the data in the form of Stanton numbers, but due to the uncertainties in determining the correct adiabatic wall temperature this does not improve the comparison between different data sets.

The heat transfer measured on the roughness elements and immediately downstream is shown in Fig. 12. The results obtained with the large cavities cannot be compared directly with the other data because of lower total temperatures during this experiment. The increase in heat transfer is, therefore, best judged by comparing the values immediately behind the roughness with the level seen farther downstream. A number of observations can be made from these results. The large cavities were subject to heating rates comparable to the undisturbed smooth wall boundary layer for the surfaces inside the cavities and up to 20% higher at the upstream edge of an upper surface. The small cavities reveal significantly higher surface heating, up to twice the undisturbed values. The largest peaks were observed with the sawtooth roughness, reaching as much as three times the undisturbed heat transfer at the outer edges. The value of $\dot{q}$ at the base of the grooves was lower than for the undisturbed boundary layer. The extreme values of heat transfer observed at the edges of the roughnesses are subject to measurement errors due to cross conduction.[3,7] The actual peak values may, therefore, lie above the results presented here. For all types of roughness an area of increased heat transfer can be seen just downstream of the last roughness element. This increase in heat transfer is limited to a short distance of about 10 mm ($\approx 1\delta_0$), after which the normal surface heat transfer is reestablished.

Figure 13 compares the heat transfer rates downstream of the roughnesses and on the 15-deg flare. An overshoot in $\dot{q}$ just downstream of the hingeline can clearly be seen for all cases. The increased heat transfer levels are limited to an area between the hingeline and 5 mm downstream, this is the equivalent of half a boundary-layer thickness in terms of the upstream boundary layer. This peak is largest for the smooth surface case. The sawtooth roughness has the smallest overshoot compared to the heat transfer upstream of the hingeline. As before, the large cavity case lies below the other configurations due to variations in flow conditions.

The measured heat-transfer on the 20-deg flare is given in Fig. 14. The results are similar to the 15-deg case, but the differences in the level of $\dot{q}$ are increased. Most of the experiments leading to these results have been subject to significant variations in surface temperature and tunnel operating conditions. The peak heat transfer near the hingeline is increased in comparison with the smaller flare. A distinct rise in heat transfer in the smooth case can also be seen at the downstream end of the model, where parts of the nozzle shock system impinge on the flare. The differences caused by the roughnesses are limited to a small reduction in peak heat transfer and a slight increase in the upstream influence.

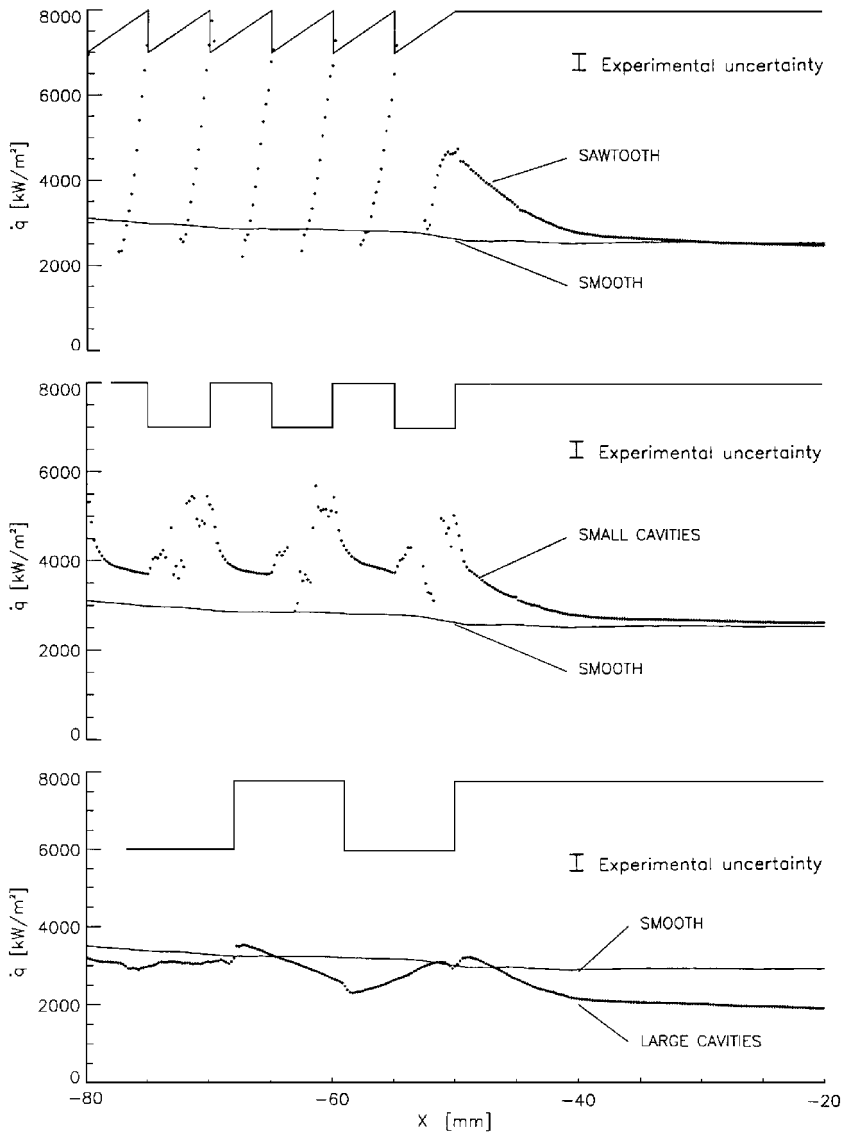

Fig. 12 Surface heat transfer distribution in the vicinity of roughness.

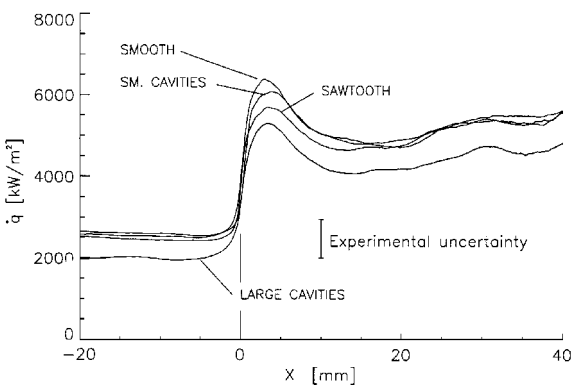

Fig. 13 Heat transfer distribution on cylinder and 15-deg flare.

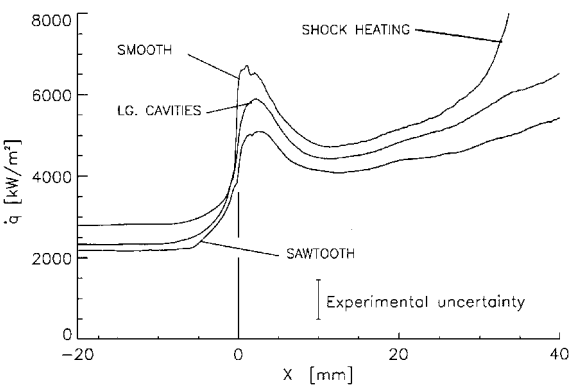

Fig. 14 Heat transfer distribution on cylinder and 20-deg flare.

When comparing the heat transfer distributions with the surface pressure measurements shown in Figs. 6 and 7, it can be seen that the increase in heat transfer and wall pressure through the corner interaction is very different in shape. This result is surprising, as it is generally assumed in turbulent hypersonic compression corners that both quantities will exhibit a similar behavior for this type of flow, as found in Refs. 8 and 9. In the cases presented here, however, the heat transfer distribution shows a rapid increase and an overshoot, whereas the surface pressure rises only slowly without reaching a plateau within the range of the measurements. It is thought that this is caused by a small-scale separation in the corner.[10]

Conclusions

The effects of a short stretch of large-scale regular surface roughness on a turbulent boundary layer and subsequent compression corner have been investigated. The types of roughness were of sawtooth and cavity shape with typical heights between half and a full boundary-layer thickness. All experiments have been performed on

axisymmetric models at Mach 5 on a turbulent boundary layer grown along the centerbody of a contoured nozzle.

The heat transfer in the rough area was found to be significantly larger than the smooth wall values. The highest peaks in heat transfer were measured on the tip of the sawtooth shaped roughness with up to three times the smooth wall results.

Downstream of the roughness each flow property exhibited a different behavior. Surface pressures were found to be uninfluenced by the roughnesses. Surface skin friction was reduced by up to 20% compared to the smooth wall value. With increasing distance from the roughness, the profiles became fuller and the differences in skin friction decreased. However, the influence of the roughness could be observed well downstream ($>10\delta_0$), even after the corner interaction. The roughnesses were found to increase the boundary-layer thickness by up to 3% and decrease the amount of fullness of the boundary-layer profiles. Roughness was found to reduce the area of validity of the log-law. The surface heat transfer behind the roughness was found to be significantly increased. Within 1.5 boundary-layer thicknesses the heat transfer returned to the undisturbed level, thus exhibiting a much shorter region of influence than skin friction. For all properties, the largest effect was observed with the sawtooth shaped roughness, whereas the small cavities had only little influence.

An approximate calculation of the drag caused by the rough region based on the momentum deficit in the boundary-layer profiles indicated the largest contribution due to the sawtooth shaped roughness and the least effect for the small cavities. The increase in drag is not consistent with the measured reduction in surface skin friction downstream of the roughness. It is, therefore, believed that the majority of the drag is caused by a different mechanism, that is, of profile drag.

The introduction of roughness had only little effect on the flow features at the compression corner. The pressures on the flare were reduced by the roughnesses, and the upstream influence was slightly increased. It is believed that the reduction in pressure increase due to roughness is caused by the decrease in velocities in the outer part of the velocity profile and the thickening of the boundary layer. Even though the reduction of velocity close to the surface is visible in the profiles for some time, the relaxation on the smooth surface upstream of the hingeline is sufficient to limit the roughness effect on the interaction. This differs from other studies, which investigated rough compression corner flows and found a significant effect of roughness on interaction length even for flows that were far from separation in the smooth wall case.

References

[1]Disimile, P. J., and Scaggs, N. E., "Turbulent Boundary-Layer Characteristics over a Flat Plate/Wedge Configuration at Mach 6," *AIAA Journal*, Vol. 30, No. 1, 1992, pp. 270–272.

[2]Monta, W. J., and Czarnecki, K. R., "Drag due to Two-Dimensional Surface Roughness on an Ogive Cylinder at Mach Numbers of 1.61 and 2.01," NASA TN D-2048, Dec. 1963.

[3]Babinsky, H., "A Study of Roughness in Turbulent Hypersonic Boundary-layers," Ph.D. Thesis, College of Aeronautics, Cranfield Univ., Cranfield, England, UK, Dec. 1994.

[4]Babinsky, H., and Edwards, J. A., "The Application and Analysis of Liquid Crystal Thermographs in Short Duration Hypersonic Flow," AIAA Paper 93-0182, Jan. 1993.

[5]Babinsky, H., and Edwards, J. A., "Automatic Liquid Crystal Thermography for Transient Heat-Transfer Measurements in Hypersonic Flow," *Experiments in Fluids*, Vol. 21, No. 4, 1996, pp. 227–236.

[6]Mathews, D. C., Childs, M. E., and Paynter, G. C., "Use of Coles' Universal Wake Function for Compressible Turbulent Boundary Layers," *Journal of Aircraft*, Vol. 7, No. 2, 1970, pp. 137–140.

[7]Maise, G., and Rossi, M. J., "Lateral Conduction Effects on Heat-Transfer Data Obtained with the Phase-Change Paint Technique," NASA CR-2435, 1974.

[8]Stollery, J. L., and Coleman, G. T., "A Correlation Between Pressure and Heat-Transfer Distribution at Supersonic and Hypersonic Speeds," *Aeronautical Quarterly*, Vol. 26, Nov. 1975, pp. 304–312.

[9]Hankey, W. L., and Holden, M. S., "Two-Dimensional Shock Wave Boundary-Layer Interactions in High Speed Flows," AGARDograph 203, June 1975.

[10]Babinsky, H., and Edwards, J. A., "On the Incipient Separation of a Turbulent Hypersonic Boundary-Layer," *Aeronautical Journal*, Vol. 100, No. 996, 1996, pp. 209–214.

J. C. Adams Jr.
Associate Editor